Floquet stability analysis of a wall-bounded oscillatory flow of a viscoelastic fluid

Author: Arnau Codina*
Master en Física dels Sistemes Complexos i Biofísica.
Facultat de Física, Universitat de Barcelona, Martí i Franquès 1, 08028 Barcelona, Spain.†

Advisor: Jordi Ortín
Departament de Física de la Matèria Condensada, Universitat de Barcelona
University of Barcelona Institute of Complex Systems (UBICS)

Abstract: Oscillatory fluid flows play an important role in fluid mechanics for their long history and numerous applications. In this work we will start off from Stokes' second problem of the boundary layer adjacent to an oscillatory wall in order to study the wall-bounded zero-mean oscillatory flow of a viscoelastic fluid placed between two parallel plates oscillating synchronously. From related experiments on the oscillatory flow of a viscoelastic solution in a vertical tube we know that the rectilinear flow at small forcing amplitudes gives rise to a secondary flow with toroidal vortices at larger amplitudes. Our purpose is to provide a theoretical understanding of this instability in a simpler setup. We analytically solve the governing equations of the periodic base flow, and carry out a Floquet linear stability analysis of the stress and velocity fields. We apply the Galerkin spectral method to numerically solve the corresponding generalized eigenvalue problem, and provide instability thresholds in forcing amplitude for both resonant and non-resonant forcing frequencies.

I. INTRODUCTION

Oscillatory flows in channels and tubes occur in relevant physiological and engineering processes such as blood flow, respiration, and speech [1–3], and secondary oil recovery, fluid pumping, filtration, and microfluidic mixing [4–6]. The former involve complex fluids such as blood and mucus, exhibiting non-Newtonian rheological behaviours. The stability of these flows against infinitesimal disturbances is therefore of both theoretical and practical interest.

In 1845, Stokes presented a series of problems in the field of fluid dynamics. One of these (known as Stokes' second problem) is today a classical example in fluid mechanics of a non-steady flow that can be analytically solved, one that stresses the need of adequate boundary conditions to correctly reproduce the flow of the fluid. In this problem we consider an infinitely large solid wall which is placed vertically at $x = 0$ and it oscillates with velocity $U(t) = U_0 \cos(w_0 t)$ in the z direction. A Newtonian fluid occupies the semi-infinite domain $x > 0$, with its motion driven by the motion of the wall. The solution of this problem can be obtained by solving the Navier-Stokes equations with the no-slip boundary condition, such that the vertical velocity of the fluid layer adjacent to the wall is given by $U_z(x = 0, t) = U_0 \cos(w_0 t)$. The region of fluid near the wall affected by this motion is called the Stokes layer [7].

The system that we will study is a wall-bounded version of Stokes' second problem. It has two main differences: the geometry of the problem and the rheological properties of the fluid. The system consists on a semi-infinite domain of a fluid bounded in between two vertical solid walls placed at $x = -a$ and $x = a$ and oscillating synchronously with velocity $U(t) = U_0 \cos(w_0 t)$ in the z direction (vertical). In addition we will consider a viscoelastic fluid rather than a purely viscous (Newtonian) one. The fluid elasticity will give rise to a richer phenomenology, with resonances appearing at particular values of the forcing frequency ω_0.

The stability of zero-mean oscillatory flows has been extensively studied in the case of simple (Newtonian) fluids. Von Kerczek and Davis [8] examined the stability of the oscillatory Stokes layer by integration of the full time-dependent linearized disturbance equations, and predicted absolute stability within the investigated range of Re^δ (Reynolds number based on the Stokes layer thickness δ), and perhaps for all the values of Re^δ. A given wavenumber disturbance of a Stokes layer was found by these authors to be more stable than that of the motionless state (zero Reynolds number).

Akhavan et al. [9] investigated the stability of oscillatory channel flow to infinitesimal and finite- amplitude two- and three-dimensional disturbances by direct numerical simulations of the Navier-Stokes equations using spectral techniques. All infinitesimal disturbances were found to decay monotonically to a periodic steady state, in agreement with earlier Floquet theory calculations.

Blennerhassett and Bassom investigated the linear stability both of a single Stokes layer in a semi-infinite fluid domain and of the fluid flow generated between a pair of synchronously oscillating parallel plates [10, 11]. In this second case, the infinitesimal disturbance equations were studied using Floquet theory, and pseudospectral numerical methods were used to solve them. Neutral curves for different plate separations were obtained, shedding light on former conflicting results in the literature. The authors showed also that the linear stability properties of the single Stokes layer were recovered when the channel half-width, scaled by the thickness of the Stokes layer,

* arnaucodvil@gmail.com
† master.complex.biophys@ub.edu

exceeded 14.

In contrast, the stability of the viscoelastic Stokes layer and related oscillatory viscoelastic flows has not yet been studied. The simplest way to reproduce the behaviour of a viscoelastic fluid is provided by the Maxwell model. One can think of Maxwell viscoelastic behaviour as a composition of an elastic spring and a viscous damper in series. These two elements describe how the material can exhibit both solid-like and liquid-like behaviours, at short and long time scales, respectively. We will, therefore, characterize the fluid with a viscosity η and a relaxation time λ upon which the fluid will behave like a viscous liquid. For this reason we will be tackling this problem by solving the generalised Navier-Stokes equation or momentum balance equation with a single-mode Maxwell constitutive equation, and with the corresponding no-slip conditions, in this case: $U(x = \pm a, t) = U_0 \cos(w_0 t)$. This system presents a well behaved and analytical solution.

Experiments of oscillatory motion of a viscoelastic fluid in a bounded domain were done in a cylindrical geometry, where the fluid was oscillated by means of a piston at the bottom [12–14]. It was seen that for low oscillation amplitudes a stable rectilinear flow was established. However, by raising the forcing amplitude the flow underwent a transition, and a secondary flow set in which presented toroidal-like vortices along the z axis. Upon raising the forcing amplitude even higher, the flow became completely turbulent [15, 16]. In the vertical pipe the governing equations are conveniently written in cylindrical coordinates, and the rectilinear base flow is expressed in terms of Bessel functions of the first and second kind, of complex argument [17]. It is anticipated that a Floquet stability analysis of this base flow will be very cumbersome from a mathematical point of view. It is for this reason that we have chosen to deal first with the more simple problem of the oscillatory flow between two synchronous parallel plates, which admits a description in Cartesian coordinates and where the base flow is more simply given in terms of hyperbolic trigonometric functions of complex argument. It is reasonable to expect that an scenario similar to the one observed experimentally in the vertical cylinder will also take place in this more simple setup.

The goal of this work is to predict the onset of instability of the rectilinear flow as a function of the forcing frequency and amplitude. In order to do this we will apply an infinitesimal perturbation to the basic flow, and perform a linear stability analysis via the Floquet method. The partial differential equations for the perturbed stress and velocity fields will be solved numerically with a Galerkin-Legendre spectral method.

The remainder of this thesis is organized as follows: In Section II we derive the equations that govern the initial rectilinear base flow. In Section III we present the perturbations that will be imposed on the flow and find the governing equations for the perturbed flow. Section IV is devoted to explaining the Galerkin spectral method and Floquet analysis that will be implemented in order to solve the perturbed flow and analyse its stability. Our results are presented and discussed in Section V. In Section VI, finally, we draw the main conclusions of our work, and outline possible future research lines that derive from this study.

II. BASIC FLOW

The main inspiration behind this problem is Stokes' second problem, which considers an infinite flat plate beneath a semi-infinite layer of initially quiescent incompressible viscous fluid; the plate oscillates harmonically in its own plane, y–z say, along the z axis, with amplitude z_0 and angular frequency ω_0, and the purpose is to obtain the steady periodic one-dimensional flow field, $\mathbf{u}(x, t)$. In our problem, however, we further constrict the flow by adding a second flat plate parallel to the first one and at a distance of $2a$ so that the plates are placed at $x = -a$ and $x = +a$.

The flow is governed by the momentum balance equation and the continuity equation for an incompressible fluid:

$$\rho \left[\frac{\partial \mathbf{u}}{\partial t} + (\mathbf{u} \cdot \boldsymbol{\nabla}) \mathbf{u} \right] = -\boldsymbol{\nabla} p + \boldsymbol{\nabla} \cdot \boldsymbol{\tau}, \tag{1}$$

$$\boldsymbol{\nabla} \cdot \mathbf{u} = 0. \tag{2}$$

Here ρ is the density of the fluid, $\mathbf{u}(\mathbf{r}, t)$ is the flow field, p is the applied pressure, and $\boldsymbol{\tau}$ is the stress field.

To study the base flow of the problem we can assume for symmetry reasons that the only non-zero component of the flow field has direction z and depends only on x, so that

$$\mathbf{u} = (0, 0, \mathcal{U}_z(x, t)). \tag{3}$$

It is immediate to see that the incompressibility condition (2) is satisfied.

We will also use no-slip boundary conditions at the walls,

$$\mathcal{U}_z(-a, t) = \mathcal{U}_z(a, t) = z_0 \omega_0 \cos(w_0 t) = U_0 \cos(w_0 t). \tag{4}$$

The advective term in (1) is

$$(\boldsymbol{u} \cdot \boldsymbol{\nabla})\, \boldsymbol{u} = \mathcal{U}_z \frac{\partial}{\partial z} \boldsymbol{u} = 0. \tag{5}$$

The gravitational body force along z on each fluid element (not included in equation (1) for simplicity) gives rise to a vertical hydrostatic pressure gradient. There is no applied pressure gradient, however, and thus the pressure term in (1) is $\boldsymbol{\nabla} p = 0$.

In order to find a relationship between the stress tensor and the flow we can use the constitutive equation of the fluid, which relates the stress tensor $\boldsymbol{\tau}$ and the rate-of-strain tensor $\boldsymbol{e} = [\nabla \boldsymbol{u} + (\nabla \boldsymbol{u})^{\dagger}]/2$. The simplest constitutive equation for a viscoelastic fluid is given by the single-mode upper-convected Maxwell equation (UCM)

$$\boldsymbol{\tau} + \lambda \boldsymbol{\tau}_{(1)} = 2\eta \mathbf{e}. \tag{6}$$

This equation features a constant viscosity η and a single fluid relaxation time λ. The subindex (1) represents an upper-convected time derivative that makes the equation frame invariant:

$$\boldsymbol{\tau}_{(1)} = \frac{\partial \boldsymbol{\tau}}{\partial t} + (\boldsymbol{u} \cdot \nabla)\, \boldsymbol{\tau} - \left\{ (\nabla \boldsymbol{u})^{\dagger} \cdot \boldsymbol{\tau} + \boldsymbol{\tau} \cdot (\nabla \boldsymbol{u}) \right\}. \tag{7}$$

The stress tensor has, as non-zero components, the pressures and the tangential stresses that do not involve the y axis:

$$\begin{pmatrix} \tau_{xx}(x,t) & 0 & \tau_{xz}(x,t) \\ 0 & \tau_{yy}(x,t) & 0 \\ \tau_{xz}(x,t) & 0 & \tau_{zz}(x,t) \end{pmatrix}, \tag{8}$$

in which all components depend solely on the x coordinate and time.

The UCM constitutive equation (6) for every non-zero component leads to

$$\left(1 + \lambda \frac{\partial}{\partial t}\right) \tau_{xx} = 0, \tag{9}$$

$$\left(1 + \lambda \frac{\partial}{\partial t}\right) \tau_{yy} = 0, \tag{10}$$

$$\left(1 + \lambda \frac{\partial}{\partial t}\right) \tau_{xz} - \lambda \tau_{xx} \frac{\partial u_z}{\partial x} = \eta \frac{\partial u_z}{\partial x}, \tag{11}$$

$$\left(1 + \lambda \frac{\partial}{\partial t}\right) \tau_{zz} - 2\lambda \tau_{xz} \frac{\partial u_z}{\partial x} = 0. \tag{12}$$

We find that τ_{xx} and τ_{yy} exponentially decay to 0 in a time scale proportional to λ. On the other hand, τ_{xz} and τ_{zz} can be found by solving their respective equations (11) and (12) numerically. These integrations have been done using the Crank-Nicolson method, which is an implicit and stable method used in solving partial differential equations [18]. Details are provided in Appendix A. The result of the numerical integration is shown in figure 1. From figure 1 we can see that all stresses have a transient period that lasts for about $t \approx 2\lambda$ due to the elastic nature of the viscoelastic fluid before they reach a steady oscillatory regime after that time period. These results make sense since τ_{xz} is the Newtonian stress due to viscosity. This shear stress is a consequence of parallel streamlines of fluid having different velocities, thus leading to nonzero vorticity. This is reminiscent of a Kelvin-Helmholtz instability problem with an infinite number of interfaces. On the other hand, the τ_{zz} stress component is the elastic stress due to the viscoelasticity of the fluid.

Plugging the UCM constitutive equation (6) inside the momentum balance equation (1) we obtain

$$\rho \frac{\partial \boldsymbol{u}}{\partial t} = \boldsymbol{\nabla} \cdot \left(2\eta \boldsymbol{e} - \lambda \boldsymbol{\tau}_{(1)}\right), \tag{13}$$

which we can write down explicitly, to end up with the following linear partial differential equation:

$$\rho \left(1 + \lambda \frac{\partial}{\partial t}\right) \frac{\partial \mathcal{U}_z}{\partial t} - \eta \frac{\partial^2 \mathcal{U}_z}{\partial x^2} = 0, \tag{14}$$

which is the governing equation of the base flow.

It is convenient at this stage to take a small detour and rewrite equation (14) in dimensionless form. To this purpose we define the non-dimensional variables $x^* = x/a$ and $t^* = t/\lambda$, so that $\boldsymbol{u}^* = \boldsymbol{u}\lambda/a$. Equation (14) then becomes

$$\frac{1}{\mathrm{El}} \left(1 + \frac{\partial}{\partial t^*}\right) \frac{\partial \mathcal{U}_z^*}{\partial t^*} - \frac{\partial^2 \mathcal{U}_z^*}{\partial x^{*2}} = 0, \tag{15}$$

where $\mathrm{El} = \eta\lambda/\rho a^2$ is called the elasticity number. El can be interpreted as the ratio of both elastic and viscous forces to inertial forces, $\mathrm{El} = \mathrm{Wi}/\mathrm{Re}$, where $\mathrm{Wi} = U_0\lambda/a$ is the Weissenberg number, i.e. given here by the dimensionless amplitude of the oscillating plates, and $\mathrm{Re} = U_0 a\rho/\eta$ is a Reynolds number based on the size of the fluid domain.

Through the non-dimensional formulation of the balance-momentum equation (15) we can see that the dynamics of the problem depend only on the elasticity number, which in turn is given only by the dimensions of the set-up and the material properties of the fluid used.

In dimensionless form, the no-slip boundary condition (4) reads

$$\mathcal{U}_z^*(-1, t^*) = \mathcal{U}_z^*(1, t^*) = \mathrm{Wi}\cos(\mathrm{De}\, t^*), \tag{16}$$

where $\mathrm{De} = w_0\lambda$ is called the Deborah number, the dimensionless frequency of the oscillating plates. Note that both the amplitude and frequency of the oscillation influence the problem solely through the boundary condition.

In order to solve equation (15) we will assume that

$$\mathcal{U}_z^* = \mathrm{Wi} \cdot \Re(e^{i\mathrm{De}\, t^*} f(x^*)). \tag{17}$$

By substituting (17) in equation (15) and recovering the physical variables we arrive to the solution

$$\mathcal{U}_z(x,t) = U_0 \cdot \Re\left(\frac{\cosh(\kappa x)}{\cosh(\kappa a)} e^{i\omega_0 t}\right) \tag{18}$$

where $\kappa = (1/x_0) + i(2\pi/\lambda_0)$ is a complex reciprocal length scale. From the solution of Stokes' second problem for a single-mode Maxwell model, it is known that the values of x_0 and λ_0 represent the penetration length and wavelength of the transverse waves triggered by the oscillations of the boundary, and they satisfy [17, 19]

$$x_0 = \sqrt{\frac{2\eta\lambda}{\rho \mathrm{De}}} \sqrt{\frac{1}{-\mathrm{De} + \sqrt{1 + \mathrm{De}^2}}}, \tag{19}$$

$$\frac{\lambda_0}{2\pi} = \sqrt{\frac{2\eta\lambda}{\rho \mathrm{De}}} \sqrt{\frac{1}{\mathrm{De} + \sqrt{1 + \mathrm{De}^2}}}. \tag{20}$$

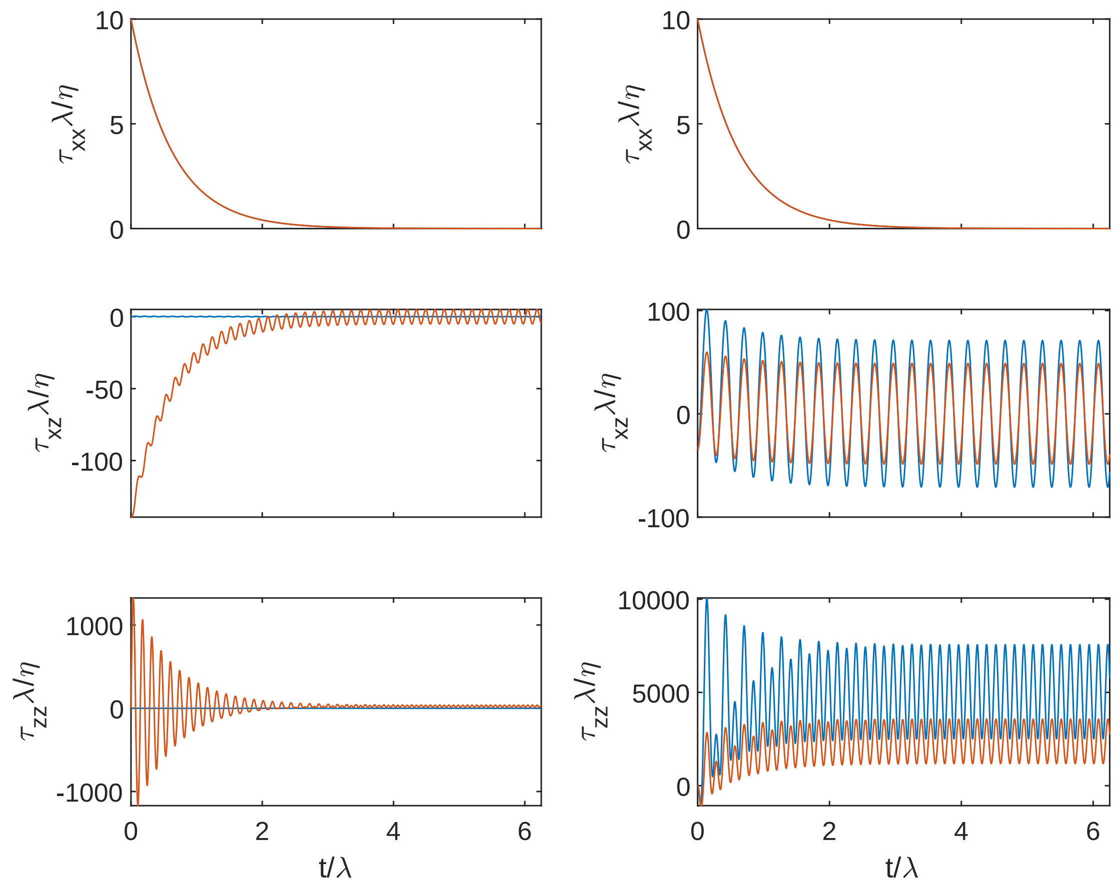

Figure 1. Representation of the τ_{xx}, τ_{xz} and τ_{zz} stress components for the basic flow as a function of time at the wall (blue curve) and halfway between the left wall and the center (orange curve) for $\mathrm{De} = 2\pi\sqrt{\mathrm{El}}$ (non-resonant condition, left panels) and for $\mathrm{De} = \pi\sqrt{\mathrm{El}}$ (resonant condition, right panels) with $\mathrm{El} = 50$. We can see how upon reaching a time of $t \approx 2\lambda$ the stresses relax and stay stationary. τ_{yy} stress components are not represented as they are decoupled from all other equations and are irrelevant to the problem due to its symmetry.

It will be useful to rewrite equation (20) in non-dimensional form by dividing both sides of the equation by a, so that λ_0^* is written in terms of the elasticity number:

$$\frac{\lambda_0^*}{2\pi} = \sqrt{\frac{2\mathrm{El}}{\mathrm{De}}}\sqrt{\frac{1}{\mathrm{De} + \sqrt{1+\mathrm{De}^2}}}. \tag{21}$$

For $\mathrm{De} > 5$ we can approximate $\mathrm{De}^2 + 1 \approx \mathrm{De}^2$, so that equation (21) becomes

$$\frac{\lambda_0^*}{2\pi} = \frac{1}{\mathrm{De}}\sqrt{\mathrm{El}}. \tag{22}$$

From the geometry of the problem one can see that the velocity waves will be generated simultaneously from the left and right walls, thus generating an interference pattern in the flow. Therefore, it is interesting to study both the cases of regular and constructive interference. The condition for constructive interference or resonance is $2a = (1/2 + n)\lambda_0$ with $n = 0, 1, 2, \ldots$ It is convenient to rewrite this resonance condition in non-dimensional variables, i.e. $2 = (1/2+n)\lambda_0^*$. Substituting the resonance condition in equation (22) we find the values of Deborah for which the flow is resonant. They are given by

$$\mathrm{De} = \pi\sqrt{\mathrm{El}}\left(\frac{1}{2} + n\right) \qquad n = 0, 1, 2, \ldots \tag{23}$$

At these Deborah values the peak velocity increases significantly and its phase shifts by $\pi/2$, as shown in figure 2.

III. LINEAR STABILITY ANALYSIS

From the experiments carried out in a vertical cylinder by Casanellas and Ortín we know that the laminar

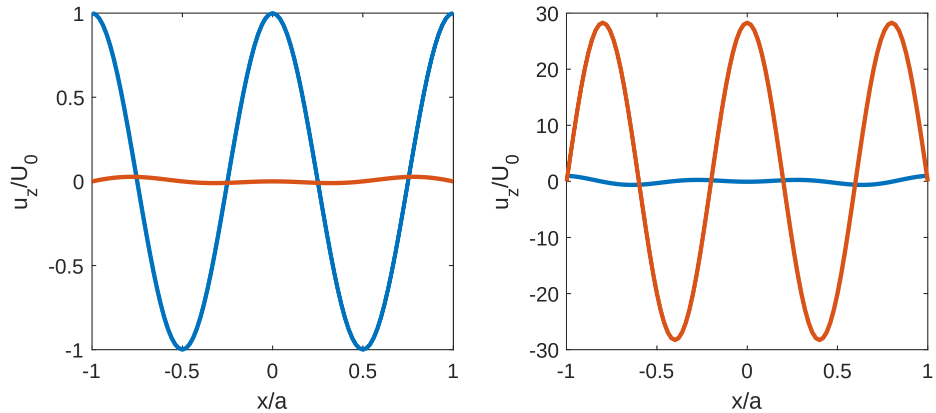

Figure 2. Vertical velocity profile of the basic flow in the oscillating wall-bounded problem for a Maxwell-like viscoelastic fluid for De= $4\pi\sqrt{\mathrm{El}}$ (non-resonant condition, left) and De= $5\pi\sqrt{\mathrm{El}}$ (resonant condition, right) with El= 50, at time phases $w_0 t = 0$ (blue curve) and $w_0 t = \pi/2$ (orange curve). Note the different vertical scales.

rectilinear flow $\mathcal{U}_z(x,t)$ became unstable against the formation of vortex rings as the forcing amplitude z_0 became sufficiently large. Moreover, the threshold amplitude of the instability was found to be highly dependent on the forcing frequency ω_0.

From the study of the base flow done on the previous section it is impossible for the flow to exhibit this kind of behaviour, as $\mathcal{U}_z(x,t)$ is a well-behaved periodical function for all x and time. Therefore, if we want to study the regime in which the rectilinear flow is not stable anymore we need to introduce some perturbations in our system.

To this purpose we will perturb the velocity in both the x and z axis and also the stress components that do not involve the y component. In all cases we are submitting the variables to an exponential perturbing mode in the z axis and let the amplitude of the perturbation depend on x and time. This way, we have:

$$\boldsymbol{U} = (u(x,z,t), 0, w(x,z,t)) = (u_p(x,z,t), 0, w_p(x,z,t) + \mathcal{U}_z) = (\tilde{u}(x,t)e^{i\alpha z}, 0, \tilde{w}(x,t)e^{i\alpha z} + \mathcal{U}_z(x,t)), \tag{24}$$

$$\boldsymbol{\tau} = \begin{pmatrix} \tau_{xx}(x,z,t) & 0 & \tau_{xz}(x,z,t) \\ 0 & \tau_{yy}(x,z,t) & 0 \\ \tau_{xz}(x,z,t) & 0 & \tau_{zz}(x,z,t) \end{pmatrix} = \begin{pmatrix} 0 & 0 & \tau^0_{xz}(x,t) \\ 0 & 0 & 0 \\ \tau^0_{xz}(x,t) & 0 & \tau^0_{zz}(x,t) \end{pmatrix} + \begin{pmatrix} T_{xx}(x,z,t) & 0 & T_{xz}(x,z,t) \\ 0 & T_{yy}(x,z,t) & 0 \\ T_{xz}(x,z,t) & 0 & T_{zz}(x,z,t) \end{pmatrix} =$$

$$\begin{pmatrix} 0 & 0 & \tau^0_{xz}(x,t) \\ 0 & 0 & 0 \\ \tau^0_{xz}(x,t) & 0 & \tau^0_{zz}(x,t) \end{pmatrix} + \begin{pmatrix} \tilde{T}_{xx}(x,t)e^{i\alpha z} & 0 & \tilde{T}_{xz}(x,t)e^{i\alpha z} \\ 0 & \tilde{T}_{yy}(x,t)e^{i\alpha z} & 0 \\ \tilde{T}_{xz}(x,t)e^{i\alpha z} & 0 & \tilde{T}_{zz}(x,t)e^{i\alpha z} \end{pmatrix} \tag{25}$$

where $\mathcal{U}_z(x,t)$ will from now on be used to indicate the base state flow of the system and τ^0_{ii} the stress components of the fluid in its base state. By using these perturbations any derivative with respect to z can be replaced by $i\alpha$.

Once we have the perturbed flows and stresses we can work as we did in section II in order to obtain the equations that govern the perturbed system. From here on, derivatives will be written as $\partial_i = \partial/\partial i$ and second derivatives will be written as $\partial_{ij} = \partial/(\partial i \partial j)$ for the sake of compactness.

We start off, yet again, with the momentum balance equation (1), the incompressibility condition (2) and the UCM constitutive equation (6).

From the incompressibility condition we can obtain a constraint between the components x and z of the perturbed velocity:

$$\partial_x \tilde{u}(x,t) + i\alpha\tilde{w}(x,t) = 0. \tag{26}$$

The advective term in (1) is no longer zero and now it reads:

$$(\boldsymbol{u}\cdot\boldsymbol{\nabla})\boldsymbol{u} = (i\alpha u_p \mathcal{U}_z, 0, u_p \partial_x \mathcal{U}_z + i\alpha \mathcal{U}_z w_p). \tag{27}$$

Unlike in section II where there was only one unknown variable ($\mathcal{U}_z(x,t)$) which led to a single equation that we then solved, this problem is more complex. We arrive to a set of equations with u_p, w_p, T_{xx}, T_{xz} and T_{zz} as variables which we have to solve for. In order to maintain the problem linear, as we will be using linear stability analysis to study whether the solutions are stable or not, we will neglect terms of order higher than 1 in the perturbations. This is to say that any term with a product of two or more perturbations will be neglected.

From the UCM constitutive equation (6) we obtain three equations (29) to (31) and from the momentum balance equation

$$\rho\left[\frac{\partial \boldsymbol{u}}{\partial t} + (\boldsymbol{u}\cdot\boldsymbol{\nabla})\boldsymbol{u}\right] = \boldsymbol{\nabla}\cdot\boldsymbol{\tau} \tag{28}$$

we obtain two more equations (32) and (33).

The set of equations we obtain is the following:

$$(1+\lambda\partial_t)\tilde{T}_{xx} + i\alpha\lambda\mathcal{U}_z\tilde{T}_{xx} - 2i\alpha\lambda\tau^0_{xz}\tilde{u} + \lambda\tilde{u}\partial_x\tau^0_{xx} - 2\lambda\tau^0_{xx}\partial_x\tilde{u} = 2\eta\partial_x\tilde{u}, \tag{29}$$

$$(1+\lambda\partial_t)\tilde{T}_{xz} + \lambda\tilde{u}\partial_x\tau^0_{xz} - i\alpha\lambda\tau^0_{zz}\tilde{u} - \lambda\tau^0_{xz}(\partial_x\tilde{u} + i\alpha\tilde{w}) - \lambda\tilde{T}_{xx}\partial_x\mathcal{U}_z + i\alpha\lambda\mathcal{U}_z\tilde{T}_{xz} - \lambda\tau^0_{xx}\partial_x\tilde{w} = \eta(\partial_x\tilde{w} + i\alpha\tilde{u}), \tag{30}$$

$$(1+\lambda\partial_t)\tilde{T}_{zz} + \lambda\tilde{u}\partial_x\tau^0_{zz} + i\alpha\lambda\mathcal{U}_z\tilde{T}_{zz} - 2\lambda\tau^0_{xz}\partial_x\tilde{w} - 2\lambda\tilde{T}_{xz}\partial_x\mathcal{U}_z - 2i\alpha\lambda\tau^0_{zz}\tilde{w} = 2i\alpha\eta\tilde{w}, \tag{31}$$

$$\rho(\partial_t + i\alpha\mathcal{U}_z)\tilde{u} = \partial_x\tilde{T}_{xx} + i\alpha\tilde{T}_{xz}, \tag{32}$$

$$\rho(\partial_t\tilde{w} + \tilde{u}\partial_x\mathcal{U}_z + i\alpha\mathcal{U}_z\tilde{w}) = \partial_x\tilde{T}_{xz} + \partial_z\tilde{T}_{zz}, \tag{33}$$

where the terms satisfying the corresponding equations for the base flow, and a global factor $e^{i\alpha z}$, have been removed. In order to tackle this system of equations we start off by defining the non-dimensional variables $x^* = x/a$, $z^* = z/a$, $t^* = t/\lambda$. Then, $\tilde{u}^* = \tilde{u}\lambda/a$, $\tilde{w}^* = \tilde{w}\lambda/a$, $\mathcal{U}^*_z = \mathcal{U}_z\lambda/a$ and $\alpha^* = \alpha a$. In order to make the stresses non-dimensional we can choose between viscosity-driven or inertia-driven variables. For this problem we have chosen the non-dimensional stresses to be $\tau^* = \tau\lambda/\eta$, as the problem is dominated by viscous and elastic forces. Equations (29) to (33) become:

$$\hat{\mathcal{T}}\tilde{T}^*_{xx} - (2i\alpha^*\tau^{0*}_{xz} + 2\partial_{x^*})\tilde{u}^* = 0, \tag{34}$$

$$\hat{\mathcal{T}}\tilde{T}^*_{xz} + (\partial_{x^*}\tau^{0*}_{xz} - i\alpha^*\tau^{0*}_{zz} - \tau^{0*}_{xz}\partial_{x^*} - i\alpha^*)\tilde{u}^* - \tilde{T}^*_{xx}\partial_{x^*}\mathcal{U}^*_z - (i\alpha^*\tau^{0*}_{xz} + \partial_{x^*})\tilde{w}^* = 0, \tag{35}$$

$$\hat{\mathcal{T}}\tilde{T}^*_{zz} + \tilde{u}^*\partial_{x^*}\tau^{0*}_{zz} - 2(\tau^{0*}_{xz}\partial_{x^*} + i\alpha^*\tau^{0*}_{zz} + i\alpha^*)\tilde{w}^* - 2\tilde{T}^*_{xz}\partial_{x^*}\mathcal{U}^*_z = 0, \tag{36}$$

$$\frac{1}{\mathrm{El}}(\partial_{t^*} + i\alpha^*\mathcal{U}^*_z)\tilde{u}^* = \partial_{x^*}\tilde{T}^*_{xx} + i\alpha^*\tilde{T}^*_{xz}, \tag{37}$$

$$\frac{1}{\mathrm{El}}(\partial_{t^*}\tilde{w}^* + \tilde{u}^*\partial_{x^*}\mathcal{U}^*_z + i\alpha^*\mathcal{U}^*_z\tilde{w}^*) = \partial_{x^*}\tilde{T}^*_{xz} + i\alpha^*\tilde{T}^*_{zz}, \tag{38}$$

where $\hat{\mathcal{T}} = (1 + \partial_{t^*} + i\alpha^*\mathcal{U}^*_z)$, and we recover that $\mathrm{El} = \eta\lambda/(\rho a^2)$ is the elasticity number. From here on we will drop the asterisks for simplicity. We have chosen homogeneous Dirichlet and Neumann boundary conditions for the velocities, so that

$$\begin{aligned} u_p(x=\pm1,z,t) &= 0, \quad u'_p(x=\pm1,z,t) = 0,\\ w_p(x=\pm1,z,t) &= 0, \quad w'_p(x=\pm1,z,t) = 0, \end{aligned} \tag{39}$$

and no boundary conditions have been imposed on the perturbed stresses. The prime in $u'(x,z,t)$ indicates a derivative with respect to x.

It is important to note that in order to solve these equations we need the stable base flow and stresses. Therefore we will set the τ_{xx} stress to 0 and we will analytically solve equations (11) and (12) with independence of the initial conditions, as we are not interested in the initial transient phase and will need a higher precision than what we can obtain using the Crank-Nicolson approximation. Details are provided in Appendix B.

IV. GALERKIN SPECTRAL METHODS

The purpose now is to integrate equations (34) - (38) in space and time, and study the growth or decay of the perturbations in one period of oscillation. This cannot be done analytically. In order to integrate the equations with the highest possible precision, we will make use of the Galerkin spectral method [20]. This method transforms our problem from a continuous differential equation problem to a discrete one by expanding our variables on a basis of Legendre polynomials. We will then write the problem in the form

$$\dot{\boldsymbol{Z}} = \hat{L}\boldsymbol{Z} \tag{40}$$

in where $\boldsymbol{Z}$ is the Legendre expansion of $\boldsymbol{Z} = (T_{xx}, T_{xz}, T_{zz}, u_p, w_p)^T$ and $\hat{L}$ is a 5N × 5N operator matrix in which N is equal to the number of points in space in which we will be solving our equations. The overdot stands for the time derivative. Once this is done we will integrate $\boldsymbol{Z}$ over a time period using a Runge-Kutta method in order to study the stability of the problem through Floquet theory. By using a Poincare map in all N positions chosen we will be able to determine the linear stability of the base flow against the applied perturbations.

We first define a Hilbert space in our domain with internal product

$$(\boldsymbol{u}, \boldsymbol{v}) = \int_{-1}^{1} \overline{\boldsymbol{u}} \cdot \boldsymbol{v}\, dx \tag{41}$$

where the overbar denotes the complex conjugate.

We can define the Legendre polynomials of degree n $P_n(x)$ as a system of complete and orthogonal polynomials such that

$$\int_{-1}^{1} P_n(x)P_m(x)\, dx = 0 \quad \text{if } n \neq m \tag{42}$$

with a standardization condition that $P_n(1) = 1\ \forall n$. From here we can construct all the polynomial system so that $P_0(x) = 1$, $P_1(x) = x$, and for higher order polynomials we use Bonnet's recursion formula

$$(n+1)P_{n+1}(x) = (2n+1)xP_n(x) - nP_{n-1}(x). \tag{43}$$

From here we will discretize the integrals in equation (41) using the Gauss-Legendre quadratures [21] so that

$$\int_{-1}^{1} f(x)dx \approx \sum_{i=1}^{N} w_i f(x_i), \tag{44}$$

where N is the number of sample points that are used, w_i the quadrature weights, and x_i the roots of the nth Legendre polynomial. The weights are obtained through the formula

$$w_i = \frac{2}{(1-x_i^2)[P_n'(x_i)]^2}. \tag{45}$$

We define our Legendre expansions Φ as

$$\Phi_m = (1-x^2)^2 L_m(x). \tag{46}$$

Therefore we can write

$$\boldsymbol{Z} = \begin{pmatrix} T_{xx} \\ T_{xz} \\ T_{zz} \\ u \\ w_p \end{pmatrix} = \sum_{m=0}^{M-1} a_m(t) \begin{pmatrix} \Phi_m(x) \\ 0 \\ 0 \\ 0 \\ 0 \end{pmatrix} + b_m(t) \begin{pmatrix} 0 \\ \Phi_m(x) \\ 0 \\ 0 \\ 0 \end{pmatrix} + c_m(t) \begin{pmatrix} 0 \\ 0 \\ \Phi_m(x) \\ 0 \\ 0 \end{pmatrix} + d_m(t) \begin{pmatrix} 0 \\ 0 \\ 0 \\ i\alpha\Phi_m(x) \\ -\partial_x\Phi_m(x) \end{pmatrix}$$

$$\boldsymbol{Z} = a_m(t)\Phi_m^{(1)}(x) + b_m(t)\Phi_m^{(2)}(x) + c_m(t)\Phi_m^{(3)}(x) + d_m(t)\Phi_m^{(4)}(x). \tag{47}$$

The first three terms of $\boldsymbol{Z}$ are the direct polynomial decomposition of the perturbed stresses, whereas the fourth term includes both the x and z components of the perturbed velocity in order to make sure that we satisfy the incompressibility condition given by equation (26). Equations (34) to (38) can be written as $\dot{\boldsymbol{Z}} = \hat{L}\boldsymbol{Z}$, where $\hat{L}$ is a 5N×5N matrix whose matrix elements $\hat{L}_{ij}$ are N×N operator matrices such that $\dot{Z}_i = \hat{L}_{ij}Z_j$. Through the approximation done in equation (47) $\boldsymbol{Z}$ has a vector representation

$$[a_0^{(1)}, a_1^{(1)}, ..., a_{\mathrm{M}-1}^{(1)}, a_0^{(2)}, ..., a_{\mathrm{M}-1}^{(2)}, ..., a_{\mathrm{M}-1}^{(4)}]_{\Phi_\mathrm{m}^{(1)},...,\Phi_\mathrm{m}^{(4)}}$$

in a 2M dimensional space S_M with basis

$$S_M = \{\Phi_0^{(1)}, \Phi_1^{(1)}, ..., \Phi_{\mathrm{M}-1}^{(1)}, \Phi_0^{(2)}, ..., \Phi_{\mathrm{M}-1}^{(2)}, ..., \Phi_{\mathrm{M}-1}^{(4)}\}.$$

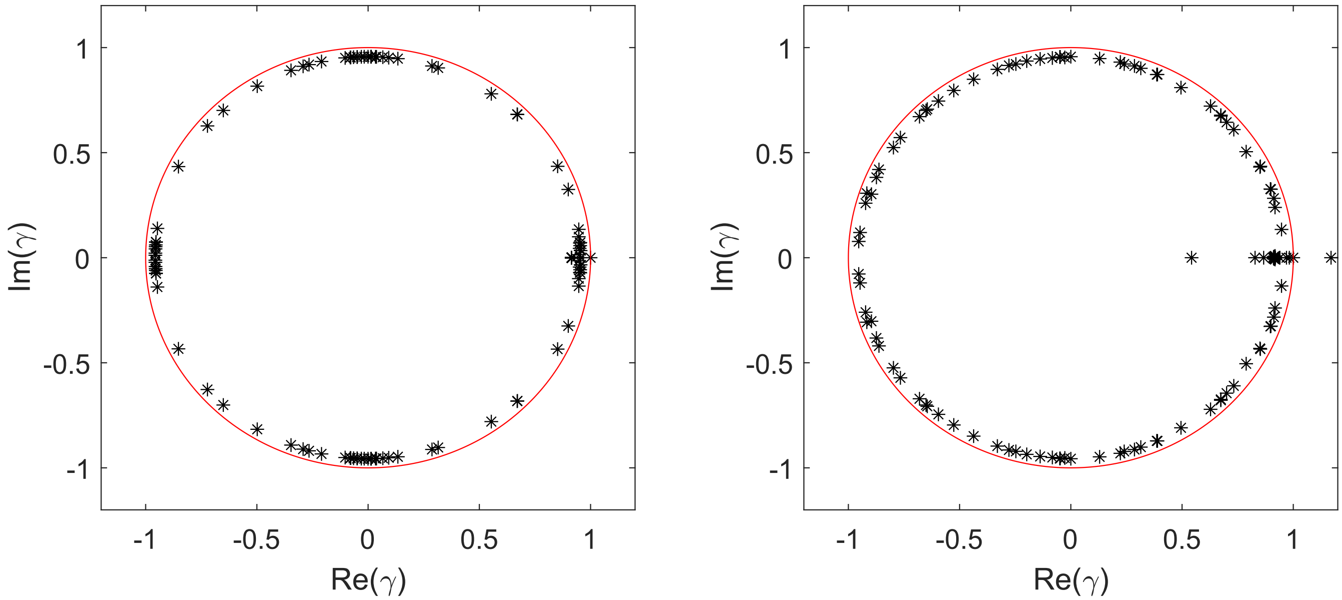

Figure 3. Representation of the Floquet exponents on the complex plane. A unit radius circumference has also been represented in order to evaluate the stability of the solutions. The figure on the left has all Floquet exponents inside the circumference so, as all of them have modulus smaller than 1, the solution is stable. On the other hand, the figure on the right has a Floquet exponents outside the circumference crossing through the real axis. As this exponent has a modulus larger than 1 this solution is unstable.

The Galerkin method consists of expanding all variables as done in equation (47) and projecting over the elements of the S_M base, so that

$$(\Phi_l^{(i)}, \dot{\boldsymbol{Z}}) = (\Phi_l^{(i)}, \hat{L}\boldsymbol{Z}) \text{ for } i = 1, ...4, \tag{48}$$

$$\sum_{m=0}^{\mathrm{M}-1} \dot{a}_m(\Phi_l^{(i)}, \Phi_m^{(1)}) + \dot{b}_m(\Phi_l^{(i)}, \Phi_m^{(2)}) + ... = \sum_{m=0}^{\mathrm{M}-1} a_m(\Phi_l^{(i)}, \hat{L}\Phi_m^{(1)}) + b_m(\Phi_l^{(i)}, \hat{L}\Phi_m^{(2)}) + ... \text{ for } i = 1, ...4, \tag{49}$$

in which $(\Phi_l^{(i)}, \Phi_m^{(j)}) = 0$ for $i \neq j$. All internal products will then be carried out computationally using equations (41) and (44). We will define the vector of Legendre coefficients $\boldsymbol{V} = (a_0, ...a_{M-1}, b_0, ..., d_{M-1})^T$. Once all the internal products have been done we are left with the following system

$$\hat{A}\dot{\boldsymbol{V}} = \hat{B}\boldsymbol{V} \qquad \Rightarrow \qquad \dot{\boldsymbol{V}} = \hat{A}^{-1}\hat{B}\boldsymbol{V}, \tag{50}$$

in which $\hat{A}$ is the operator resulting from the $(\Phi_l^{(i)}, \Phi_m^{(j)})$ internal products and $\hat{B}$ is the operator resulting from the $(\Phi_l^{(i)}, \hat{L}\Phi_m^{(j)})$ internal products.

From here we will integrate equation (50) in time during a time period using the explicit Runge-Kutta (4,5) method. Let $\hat{C} = \hat{A}^{-1}\hat{B}$, where $\hat{C}$ is a matrix with an explicit temporal dependence. Following Floquet theory one can solve equation (50) assuming an initial condition $\boldsymbol{V}(t = 0) = \mathbb{I}$. The integration process is done by individually evolving each element of the S_M base over a time period.

The result is the monodromy matrix, which is the evaluation of the fundamental matrix after a time period. The eigenvalues of the monodromy matrix are the Floquet exponents $\gamma \in \mathbb{C}$, which determine the stability of the solution. If all the exponents are confined in the radius unit circle in the complex plane, the solution is stable. If any of the Floquet exponents has modulus greater than one, the solution will have become unstable to the perturbation.

From the problem's setup, we have two main variables we can control in order to favour or disfavour the emergence of instabilities. These are the Deborah number and the Weissenberg number which correspond to the non-dimensional frequency and amplitude of oscillation respectively. The process will therefore be repeated for

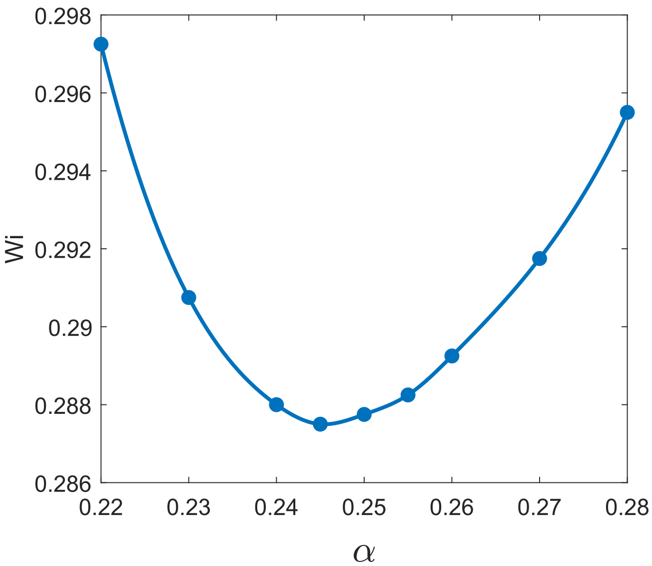

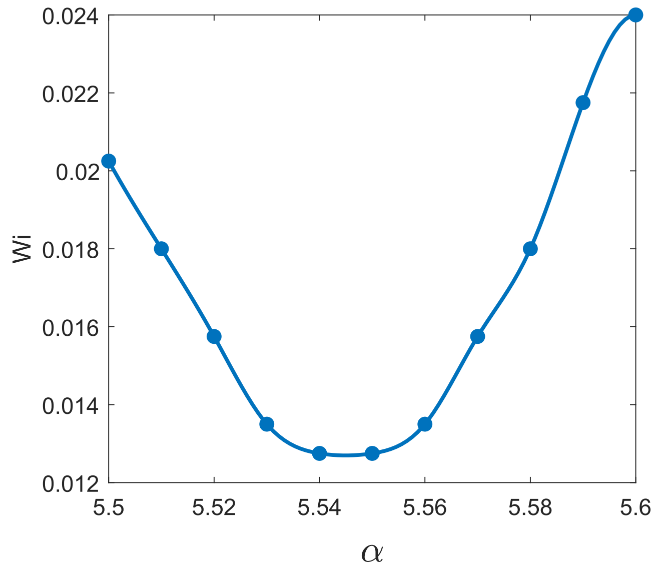

Figure 4. Representation of the neutral stability curves for a non-resonant value of Deborah (left) and a resonant value of Deborah (right). Note the difference in both the critical values of Wi and α as they both differ by an order of magnitude in those two cases. The curve serves as a stability threshold: the flow is stable for values of Wi and α under the curve and unstable for values of Wi and α above it.

any different values of Deborah, Weissenberg, and α. The aim is to find the instability threshold for different values of De. By scanning systematically the Weissenberg number for a given De, we will obtain the neutral instability curve α vs Wi for that particular De. The critical mode will be the value of α that minimizes the Weissenberg number, and the corresponding Wi will be the instability threshold for the particular value of De chosen.

After integrating equation (50) and diagonalizing the monodromy matrix we obtained the Floquet exponents. We expect that these eigenvalues will be within the unit circle up to a given critical value of the Weissenberg number. The most unstable mode will be the mode α that corresponds to the lower value of Wi. At this critical point the system will become unstable and either a single eigenvalue will escape the unit circle through the real axis or a pair of complex conjugates will escape the unit circle. It is not possible for the Floquet exponents to escape the unit circle from the imaginary axis since our equations have real coefficients. For that reason all eigenvalues cannot be purely imaginary. The way in which the eigenvalues escape the unit circle is important since it dictates the type of bifurcation the system undergoes. If an eigenvalue crosses the circumference through the real axis the bifurcation will be transcritical and the largest eigenvalue will dictate the characteristic size of the vortex that appears due to the instability. If two complex conjugate eigenvalues cross the unit circle the system will undergo a Neimark-Sacker or secondary Hopf bifurcation. This first case is what we can see in figure 3 and is what occurs in our problem for both values of De.

V. RESULTS AND DISCUSSION

Results of the stability analysis have been obtained for two cases, a resonant Deborah number ($\mathrm{De} = (5\pi/2)\sqrt{\mathrm{El}}$) and a non-resonant Deborah number ($\mathrm{De} = 2\pi\sqrt{\mathrm{El}}$), as calculations were very time-consuming computationally and the biggest differences in behaviour should be evident by studying the most extreme interference cases. All the analysis has been programmed in MatLab.

As stated before, the Weissenberg number is the dimensionless amplitude of the oscillating plates. Therefore, one can expect that the higher the Weissenberg number, the more likely it is to induce an instability of the flow. In a similar fashion, the Deborah number is the non-dimensional frequency. We can therefore expect that for resonant values of Deborah the stability threshold will be significantly lower, as the resonance condition implies a constructive interference of the flow waves generated from both plates. This constructive interference may be expected to magnify all instability driving processes, making it easier for the flow to become unstable at lower oscillation amplitudes.

Deciding upon the number of Legendre polynomials that should be used in order to approximate the perturbed stresses and velocities was challenging. After a series of convergence tests, a number of M=24 polynomials was chosen. This decision will be discussed later in the section, as the problem does not appear to converge with increasing number of polynomials, as it should.

Examples of a stable configuration and the latter unstable possibility can be seen in figure 3. However, since we are only interested in the threshold of instability we will only be taking into account the eigenvalue with the largest modulus since its behaviour will be enough to decide whether the solution is stable or unstable.

From figure 4 one can directly see the difference in the stability of the flow for the two cases studied. For the case of a non-resonant Deborah value (figure 4 left) the most dangerous perturbational mode α is about 20 times smaller than for a resonant Deborah value (figure 4 right). The critical Weissenberg number is also significantly higher in the absence of resonance. The non-resonant condition is universally stable up to a critical Weissenberg number $\mathrm{Wi} \approx 0.288$ whereas the critical value for the resonant condition is around 20 times smaller, with $\mathrm{Wi} \approx 0.013$.

These results are coherent with our predictions as we find instabilities in the flow for both resonant and non-resonant conditions due to the viscoelastic nature of the fluid. We can also reproduce the difference in stability of resonant and non-resonant conditions. We have shown that at a non-resonant value of Deborah the system can maintain a global stability condition up to a critical threshold that appears at a much higher Weissenberg value than for a resonant Deborah value.

These results are also compatible with the experiments that have been done in the field [12, 14]. We notice that, despite the fact that experiments were done in a cylindrical set-up, the instability appeared for all Deborah values, with lower critical Weissenberg numbers for resonant conditions.

However, even though the results obtained are satisfactory and compatible with the experimental evidence, the method used shows one important flaw that conditions the validity of the results. Solving equations (34)-(38) using a Galerkin spectral method with Legendre polynomials and a posterior temporal integration has shown to be very complex computationally. This happens as all the perturbations have to be carefully worked with in order not to create any artificial computational instabilities that might blow up the results.

Our initial approach was to solve every aspect of the problem analytically up to the temporal integration which is practically impossible to solve without using computational techniques. We decided to use an integrated MatLab function (ode45) that is based on the implicit Runge-Kutta (4,5) or Runge-Kutta-Fehlberg method. The way this algorithm works, in a nutshell, is by calculating the integration with an order $\mathcal{O}(h^4)$ and an order $\mathcal{O}(h^5)$ method. The order $\mathcal{O}(h^4)$ is used as the solution while the order $\mathcal{O}(h^5)$ method estimates the error. This process allows for an adaptive time step size that is determined automatically. We chose this integrator since the adaptive time step size and the higher order error estimator should provide a more exact solution than a regular Runge-Kutta 4 or other integration methods that use a single time stepsize.

Having chosen a numerical integrator we still had to decide what the suitable number of Legendre polynomials should be used to accurately approximate the perturbed stresses and velocities. To do that we performed a convergence test. We imposed values for all possible variables: the Deborah number, the Weissenberg number and the perturbation mode α. By repeating this process for different numbers of Legendre polynomials, M, we can compare the results as a function of M. In principle we would expect the results to be ill-behaved for small values of M and gradually attain a plateau and stabilise around a constant value. We would then use the smallest possible value of M that guarantees convergence since higher values of M significantly increase the computation time. However, we can see in figure 5 that this is not what happens. Even though at a number of polynomials around $\mathrm{M} = 24$ the results seem to converge, we can see that further increase in the number of polynomials results in a steady descent of the highest eigenvalue. This can be a consequence of many things but the most possible one is that increasing the amount of polynomials increases the degree of complexity of the problem as a whole thus giving rise to further computational problems that distort the solutions. We tried to solve these computational problems by attempting to solve the temporal integration in some other ways, that will be explained in the following paragraphs, but in the end we decided to settle with this approach which we believe should theoretically end up converging given a sufficiently small time step size when integrating.

The most obvious change that could be done, in this case, would be to stop using the ode45 function and introduce a method with a fixed stepsize instead of an adaptive stepsize, as we could then make the stepsize as small as we would want it to be. This was the first thing that was tried but we quickly realised that the computational time it took for a fixed stepsize method to give coherent results that were comparable, in quality, to the ones we obtained using the adaptive stepsize was far greater. To put it into perspective, the neutral stability curves found in figure 4 took a total of 14 days to be produced in a computer provided by the university. Adding this to some previous attempts that failed due to incorrect formulation or computational issues, the results took over two months to be obtained since the correct formulation for equations (34)-(38) was found. This is to say that, even if it was possible to obtain accurate results by lowering the step size, this could take many months of computational time.

The first attempt at trying another approach to the problem was to change the beam functions by which we have approximated the perturbed stresses and velocities. Instead of using Legendre polynomials we decided to use Chebyshev polynomials [22]. These polynomials are similar to Legendre polynomials since they both are orthogonal in the $[-1, 1]$ interval. Because of this both could be used in approximating our perturbed variables. However, all weights and roots are different, so equations (43) and (45) had to be revisited. After the pertinent changes and corrections we ended up with a simplified version of

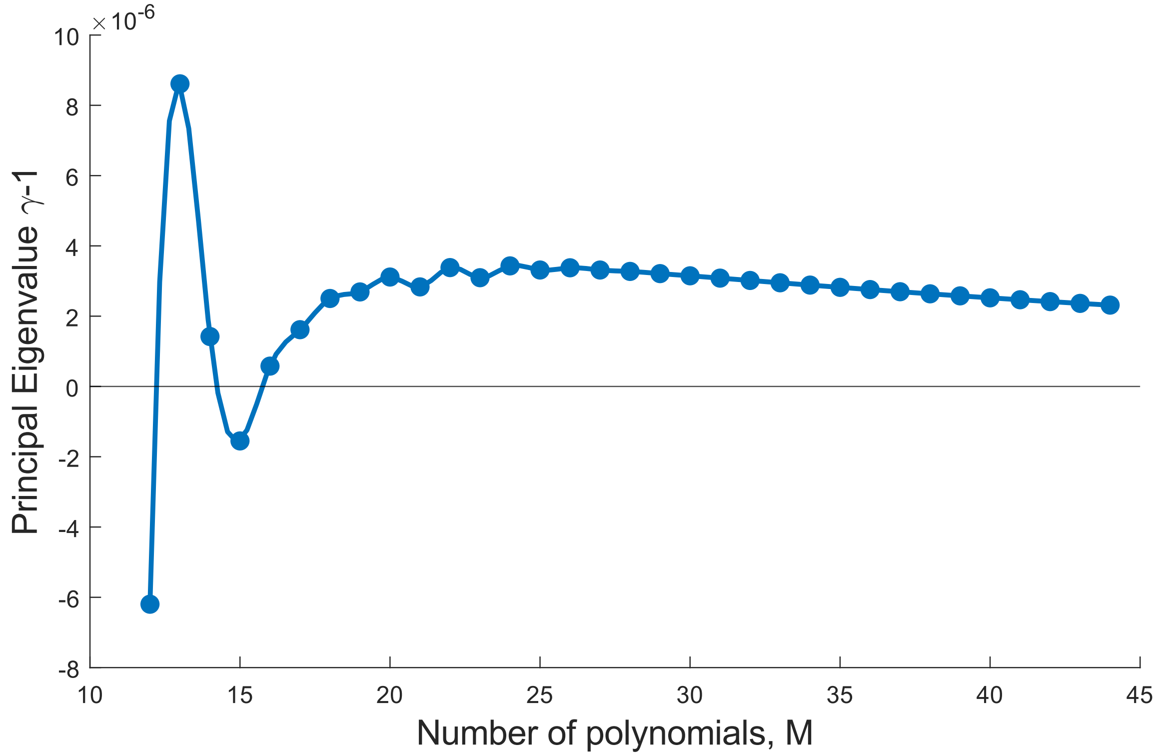

Figure 5. Convergence test of the problem for different number of Legendre polynomials used to approximate the perturbed stresses and velocities. The test was done at values of De $= 70.7468$, Wi $= 1.6$ and $\alpha = 0.7$. We are representing the value of the modulus of the biggest eigenvalue minus 1 versus the number of polynomials. We have chosen this representation so that negative values mean instability and positive values stability. We can see how for a small number of polynomials M < 20 the behaviour of the highest eigenvalue varies drastically with M. For intermediate number of polynomials $20 <$ M < 26 the value of the highest Floquet exponent seems to plateau and converge to a stable value. However, for higher number of polynomials M > 26 the value of the eigenvalue starts decreasing steadily, failing to properly converge.

equation (50) that could facilitate a more computationally efficient integration

$$\dot{\boldsymbol{V}} = \hat{B}\boldsymbol{V}, \tag{51}$$

where $\boldsymbol{V}$ and $\hat{B}$ are constructed in the same way as in equation (50) altering the value of the weights and the implementation of boundary conditions. However, after this change in formulation, the integration method that followed in order to integrate the system of equations over one period of the oscillation presented the same problems than using Legendre polynomials. For this reason we rejected using Chebyshev polynomials, since Legendre polynomials are simpler to work with.

The last attempt at solving the problem was centered around changing the time integration approach. Since both the Runge-Kutta 4 and Runge-Kutta (4,5) were blowing up at high number of polynomials we decided to solve the differential equation by exponentiating the matrix and using a temporal discretization by dividing a time period T in n discrete time steps of size dt. We start from equation (50) with initial condition $\boldsymbol{V}(t=0) = \mathbb{I}$. Let $\hat{C} = \hat{A}^{-1}\hat{B}$. From here we integrate directly and end up with

$$\boldsymbol{V}(t+1) = \exp\left(\hat{C}(t) \cdot dt\right)\boldsymbol{V}(t) \tag{52}$$

Using this recurrence relation one can find the monodromy matrix and, diagonalizing it, the Floquet exponents. Yet again, the results that were obtained with this discretization resembled those that were found using the ode45 function with the same limitations.

Since none of the attempts to make the method converge seemed to show any signs of working properly, we ultimately decided to go on with the ode45 MatLab function. From figure 5 we decided to set the amount of polynomials to M $= 24$, since this value lies in the range of values that seem to reach a plateau and since a higher value of M would be computationally too time-consuming.

Even if the method does not seem to converge, the results obtained are coherent both with our predictions and with the experiments. For this reason it seems reasonable to assume that the results may be qualitatively correct. That is to say that our results should capture the nature of the instability accurately. Even if the exact values of the critical Weissenberg number and perturbation mode α are probably quantitatively inaccurate, it seems plausible to assume that the critical Weissenberg number is lower and the critical perturbed mode α is higher at a resonant De value than at a non-resonant one.

The source of the difficulties that we have faced to integrate the system of equations defining our linear stability problem, in contrast to similar approaches for corresponding Newtonian flows, might be found in the hyperbolic nature of the terms in the differential equations coming from the elasticity of the fluid, in contrast with the parabolic nature of the typical laplacian terms in the case of a purely viscous fluid. This important difference and its consequences would deserve a deeper study, that falls however beyond the scope of this Thesis.

VI. CONCLUSIONS

Having discussed the limitations of the method used in solving our problem, we still believe that some meaningful conclusions can be extracted from the work done. The equations that govern the perturbed flow have been derived from the momentum balance and continuity equations via the upper-convected Maxwell model. Its further study and attempts in solving them also give some qualitative knowledge of the behaviour of the flow.

Before attempting to solve the equations we made a couple of assumptions. First, we thought that the initially rectilinear flow would undergo a transition and give rise to a secondary flow with the emergence of loop-shaped vortices. We thought this transition would happen for any given frequency of oscillation at a sufficiently large oscillation amplitude. We also assumed that at resonant oscillating frequencies, those frequencies in which the shear waves emitted from the two facing walls would generate constructive interference, the flow would become unstable at lower forcing amplitudes, since the resonant nature of the oscillation would amplify all instability-generating mechanisms. These assumptions, supported by the experiments that have been done in similar set-ups [12], would allow us to validate any results we could find by solving the governing equations of the flow.

The main results that were found during the work can be seen in figure 4 and are coherent with both the assumptions and the experiments. We explored the behaviour of the flow in extreme cases of constructive and destructive interference in order to analyse resonant and non-resonant values of frequency. As we expected, we found that for both cases the flow would become unstable at a given critical amplitude and mode of perturbation. We also found that, for the resonant case, the necessary amplitude of oscillation before the flow became unstable was around 20 times lower than for the non-resonant case. This shows that, as predicted, the constructive interference phenomena that leads to a resonant condition amplifies all instability driving mechanisms, thus resulting in an unstable flow at a lower amplitude of the oscillation. Ideally, we would have liked to explore more values of the oscillation frequency, but due to the limited time and computational resources available we had to select these two values to study.

In the future, one could try to solve the equations presented in section III by tackling the problem in a different way. Blennerhassett and Bassom [11] studied a very similar problem, namely the stability of a Newtonian fluid in an oscillating wall-bounded setup. In their work they followed a similar procedure than us, using Floquet analysis to study the stability of the flow. However, unlike most relevant works on the field done before them, they did not attempt to solve the temporal evolution of the flow using a numerical integrator as has been done in this work. Instead, they discretized time as well as space using Fourier series expansions and made the system evolve from a set of initial conditions.

ACKNOWLEDGMENTS

I would like to express my deepest gratitude to my advisor, Jordi Ortín, for his guidance and assistance throughout this project and without whom this work would not have been possible.

I would also like to extend my gratitude to Àlvar Meseguer and Francisco Marquès for their helping me these months with the different numerical techniques that have been implemented.

Finally, I would like to thank my family and friends for their continuous support.

[1] Ku, D.N. (1997). “Blood flow in arteries,” Annu. Rev. Fluid Mech. 29, 399–434.

[2] Grotberg, J.B. (2001). “Respiratory fluid mechanics and transport processes,” Annu. Rev. Biomedical Engineering 3, 421–457.

[3] Mittal, R., Erath, B.D., and Plesniak, M.W. (2013). “Fluid dynamics of human phonation and speech,” Annu. Rev. Fluid Mech. 45, 437–467.

[4] Margot, G. G. and Durlofsky, L. J. (2005). “Modeling fluid flow in oil reservoirs,” Annu. Rev. Fluid Mech. 37, 211–238.

[5] Jaffrin, M. Y. (2012). “Hydrodynamic techniques to enhance membrane filtration,” Annu. Rev. Fluid Mech. 44, 77–96.

[6] Selverov, K.P. and Stone, H.A. (2001). ”Peristaltically driven channel flows with applications towards micromixing”, Phys. Fluids 13, 1837-1859.

[7] Balmforth, N.J., Forterre, Y., and Pouliquen, O. (2009).

The viscoplastic Stokes layer. Journal of Non-Newtonian Fluid Mechanics, **158**, 46-53.

[8] Von Kerczek, C. and Davis, S.H. (1974). "Linear stability theory of oscillatory Stokes layers," J. Fluid Mech. 62, 753-773.

[9] Akhavan, R., Kammz, R. D., and Shapiro, A.H. (1991). "An investigation of transition to turbulence in bounded oscillatory Stokes flows Part 2. Numerical simulations," J. Fluid Mech. 225, 423-444 .

[10] Blennerhassett, P.J. and Bassom, A.P. (2002). The linear stability of flat Stokes layers. J. Fluid Mech. **464**, 393-410.

[11] Blennerhassett, P.J. and Bassom, A.P. (2002). The linear stability of high-frequency oscillatory flow in a channel. J. Fluid Mech. **556**, 1-25.

[12] Casanellas, L. (2013) Oscillatory pipe flow of wormlike micellar solutions [PhD Thesis, Universitat de Barcelona]

[13] Torralba, M., Castrejón-Pita, J., Castrejón-Pita, A., Huelsz, G., del Río, J., and Ortín J. (2005). Measurements of the bulk and interfacial velocity profiles in oscillating Newtonian and Maxwellian fluids. Phys. Rev. E **72**, 016308.

[14] Casanellas, L., and Ortín, J. (2012). Experiments on the laminar oscillatory flow of wormlike micellar solutions, Rheol. Acta **51**, 545–557.

[15] Torralba, M., Castrejón-Pita J., Hernández, G., Huelsz, G., del Río, J., and Ortín, J. (2007). Instabilities in the oscillatory flow of a complex fluid. Phys. Rev. E **75**, 056307.

[16] Casanellas, L., and Ortín, J. (2014). Vortex ring formation in oscillatory pipe flow of wormlike micellar solutions. J. Rheol. **58**, 149-181.

[17] Casanellas, L., and Ortín, J. (2011). Laminar oscillatory flow of Maxwell and Oldroyd-B fluids: Theoretical analysis. J. Non-Newtonian Fluid Mech. **166**, 1315–1326 (2011).

[18] Crank, J., and Nicolson, P. (1996). A practical method for numerical evaluation of solutions of partial differential equations of the heat-conduction type. Adv Comput Math 6, 207–226

[19] Ortín, J. (2020). Stokes layers in oscillatory flows of viscoelastic fluids. Philosophical Transactions of the Royal Society A: Mathematical, Physical and Engineering Sciences **378**, 20190521. The Royal Society.

[20] Gottlieb, D., and Orszag, S. A. (1977). Numerical Analysis of spectral methods: Theory and applications. Society for industrial and applied mathematics.

[21] Canuto, C. G., Hussaini, M. Y., Quarteroni, A., and Zang, T. A. (2007). Spectral methods: Evolution to complex geometries and applications to fluid dynamics. Springer-Verlag GmbH.

[22] Meseguer, A. (2020). Fundamentals of numerical mathematics for physicists and Engineers. John Wiley & Sons, Inc.

APPENDIX A

In order to integrate equations (9), (11) and (12), we will create a grid in time and space (using non-dimensional variables) with time step $\Delta t = 0.001$ and fitting points in the x axis $\{x\} = (x_1, x_2, ..., x_n)$ (as the stresses do not depend on y or z) that will be useful when attempting to solve the final equations. We can then approximately write equations (9), (11) and (12) as

$$\tau_{xx,i}^{n+\Delta t} = \left(1 + \frac{\Delta t}{2}\right)^{-1} \left[\tau_{xx,i}^{n} - \frac{\Delta t}{2}\tau_{xx,i}^{n}\right] \tag{53}$$

$$\tau_{xz,i}^{n+\Delta t} = \left(1 + \frac{\Delta t}{2}\right)^{-1} \left[\tau_{xz,i}^{n} + \frac{\Delta t}{2}\left(\partial_x u_{z,i}^{n+\Delta t} - \tau_{xz,i}^{n} + \partial_x u_{z,i}^{n}\right)\right] \tag{54}$$

$$\tau_{zz,i}^{n+\Delta t} = \left(1 + \frac{\Delta t}{2}\right)^{-1} \left[\tau_{zz,i}^{n} + \frac{\Delta t}{2}\left(2\tau_{xz,i}^{n+\Delta t}\partial_x u_{z,i}^{n+\Delta t} - \tau_{zz,i}^{n} + 2\tau_{xz,i}^{n}\partial_x u_{z,i}^{n}\right)\right] \tag{55}$$

where the subscript i represents the point in space ($i = x_1, x_2, ..., x_n$) and the superscript n represents the point in time ($n = 0, \Delta t, 2\Delta t, ...$). By iterating equations (54) and (55) in space and time we will be able to obtain the solutions in the desired points in space for all times. In order to do so, we will need to set the initial conditions. We have chosen that, for $t = 0$, we will use the stress values for a Newtonian fluid. To do so we solve equations (11) and (12) setting $\lambda = 0$ at $t = 0$ and obtain

$$\tau_{xz}(x, t = 0) = \partial_x u_z(x, t = 0) \tag{56}$$

$$\tau_{zz}(x, t = 0) = 0 \tag{57}$$

as our initial conditions. For equation (9) we have chosen an arbitrary initial value as the aim of figure 1 was to show the decay of the τ_{xx} stress.

APPENDIX B

In order to solve equations (11) and (12) analytically to use these solutions when using a Runge-Kutta integration we will ignore the initial transient phase.

We will first solve the following differential equation that will serve as guidance

$$(1+\lambda\partial_t)v = A_0 + A_1\cos\omega t + A_2\sin\omega t. \tag{58}$$

We will consider solutions of the form

$$v(t) = C_0 + C_1\cos\omega t + C_2\sin\omega t. \tag{59}$$

By substituting in equation (58) and solving we obtain

$$C_0 = A_0, \quad C_1 = \frac{A_1 - \lambda\omega A_2}{1+\lambda^2\omega^2}, \quad C_2 = \frac{\lambda\omega A_1 + A_2}{1+\lambda^2\omega^2} \tag{60}$$

We will now start solving for the stresses

$$(1+\lambda\partial_t)\tau_{zx} = -\eta\partial_x u_z. \tag{61}$$

To solve it we will need to rewrite the base flow in the following ways:

$$u_z(x,t) = U_0\Re\Big(\frac{\cosh\kappa x}{\cosh\kappa a}e^{i\omega_0 t}\Big) = u_1(x)\cos\omega_0 t + u_2(x)\sin\omega_0 t. \tag{62}$$

where $u_1(x)$ and $u_2(x)$ are real functions so that

$$u_1(x) = U_0\Re\Big(\frac{\cosh\kappa x}{\cosh\kappa a}\Big), \qquad u_2(x) = -U_0\Im\Big(\frac{\cosh\kappa x}{\cosh\kappa a}\Big). \tag{63}$$

We will then rewrite equation (61) as

$$(1+\lambda\partial_t)\tau_{zx} = -\eta u_1'\cos\omega_0 t - \eta u_2'\sin\omega_0 t = f_1\cos\omega_0 t + f_2\sin\omega_0 t. \tag{64}$$

Now we have the equation in the form of equation (58) with $\omega = \omega_0$, $A_0 = 0$, $A_1 = f_1 = -\eta u_1'$ i $A_2 = f_2 = -\eta u_2'$ so its permanent solution is

$$\tau_{zx}(x,t) = D_1\cos\omega_0 t + D_2\sin\omega_0 t, \tag{65}$$

$$D_1 = \frac{f_1 - \lambda\omega_0 f_2}{1+\lambda^2\omega_0^2}, \qquad D_2 = \frac{\lambda\omega_0 f_1 + f_2}{1+\lambda^2\omega_0^2}. \tag{66}$$

We will now solve for

$$(1+\lambda\partial_t)\tau_{zz} = -2\lambda\tau_{zx}\partial_x u_z, \tag{67}$$

We substitute in expression (66) and obtain:

$$(1+\lambda\partial_t)\tau_{zz} = -2\lambda\tau_{zx}\partial_x u_z = -2\lambda(D_1\cos\omega_0 t + D_2\sin\omega_0 t)(u_1'\cos\omega_0 t + u_2'\sin\omega_0 t) \tag{68}$$

$$= g_0 + g_1\cos 2\omega_0 t + g_2\sin 2\omega_0 t, \tag{69}$$

$$g_0 = -\lambda(D_1u_1' + D_2u_2'), \quad g_1 = -\lambda(D_1u_1' - D_2u_2'), \quad g_2 = -\lambda(D_1u_2' + D_2u_1'), \tag{70}$$

Now we have the equation in the form of equation (58) with $\omega = 2\omega_0$, $A_0 = g_0$, $A_1 = g_1$ i $A_2 = g_2$. Its permanent solution is therefore:

$$\tau_{zz}(x,t) = E_0 + E_1\cos 2\omega_0 t + E_2\sin 2\omega_0 t, \tag{71}$$

$$E_0 = g_0, \qquad E_1 = \frac{g_1 - 2\lambda\omega_0 g_2}{1+4\lambda^2\omega_0^2}, \qquad E_2 = \frac{2\lambda\omega_0 g_1 + g_2}{1+4\lambda^2\omega_0^2}. \tag{72}$$